Section 7

Global and regional climate models, sensitivity and impact experiments, response to external forcing

Sensitivity of Snow Water Equivalent Distribution to Variations of Critical Snow Albedo in GCM Experiments of Hydrometcentre of Russia

Valentina M. Khan*, Konstantin Rubinstein*, Marina Zoloeva*
*- Hydrometeorological Research Center of the Russian Federation
e-mail: khan@mecom.ru

Snow is a very important component of climate system. Adequate simulation of snow cover characteristics in hydrodynamical models is one of the indicators parameterization reliability of hydrological and heat balance processes of the model. Simulation of snow cover area (SCA) at global and regional scale in AMIP - type experiments was the point of special interest in a number of publications (e.g. Frei et al. 2005). Hall & Qu, 2006, Roesch 2006 showed that snow albedo feedback is critical for climate models prediction. The objective of the present study is to examine the effects related with introducing variable critical surface albedo of snow in model which is in winter time directly depend on snow cover. Information about snow density of different class of snow was obtained from Sturm, 1995 classification approach. Then own critical value of albedo is prescribed for each class of snow cover (Tudra – 0.95, Taiga – 0.95, Maritime – 0.7, Ephemeral – 0.5, Prairie – 0.76, Mountain – 0.87). In the model was introduced procedure of counting dynamics of snow classes, depending on three month mean surface air temperature, precipitation and wind. According to class of snow cover these critical snow albedo values were introduced for experiment. For comparison, in model control run the critical value of surface snow albedo is assumed as a constant (0.8). In this study the SWE parameter is validated as effect of varying of snow critical albedo on the surface.

Before evaluation process of model SWE data, we investigated which of is snow data set can be used as etalon for evaluation of model. There is no global snow water equivalent and snow depth datasets with good spatial and temporal resolution. Brown et al. (2003) developed regional gridded monthly snow depth and water equivalent data set for period from 1979 to 1996 with good spatial resolution over North America region. It is not possible elaborate the same dataset at global scale due to insufficient number of observations *in situ* over other parts of the globe. In this study we verified quality of reanalysis to adequately reproduce SWE. Validation of snow water equivalent (SWE) from 4 types of reanalysis (ERA-40 (ECMWF), NCEP/NCAR, NCEP/DOE and JRA-25) against measured SWE from snow survey routs over FSU territory for period from 1979 to 2000 using several statistical criteria was performed (Khan et al., 2007). The results of comparative analysis indicated that SWE from ECMWF is the closest to observational data for mostly FSU territory. SWE from JRA-25 reanalysis is reasonably reproducing observational data since 1986. NCEP/DOE is only able adequately simulate the long-term tendencies of SWE averaged over large regions. So, the global SWE from ERA-40, ECMWF reanalysis was used for validation of outputs from GCM of Hydrometcentre of Russia.

Both GCM experiments (control and with different albedo of classes) correspond to AMIP protocol requirements. In the second experimental run the effect of varying surface albedo tend to be closer to surface albedo climatologies from remote-sensed estimations. Preliminary results indicate that seasonal variability of SWE is reproduced well in the model for both runs, although the spatial distribution in some regions contradicts with etalon data. Figure 1. demonstrates seasonal distribution of SWE averaged over North America, Europe and Asia. Results from both control and experimental runs are close to each other over large integrated areas although they can substantially diverge at separate points. Over Europe, the

seasonal variability is reproduced well by phase, but the amplitude is underestimated by model runs almost in twice. For Asia and North America, formation of snow cover is simulated very close to etalon data, but the melting processes of snow are significantly delayed. SWE from model runs overestimate SWE from ERA-40 in a range from 50%-100%.

Influence of introducing of variable critical albedo in GCM for simulation of SWE can be seen from Figure 2. Spatial distribution of RMSE of SWE from control and experimental runs exhibits geographical areas over globe most sensible to more accurate albedo description in the model.

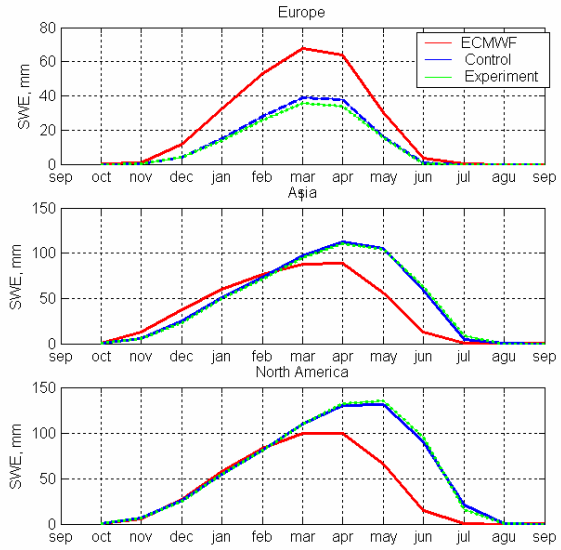

Figure1. Seasonal variability of SWE from ERA-40 reanalysis, control and albedo experiments runs averaged over Europe, Asia and North America regions

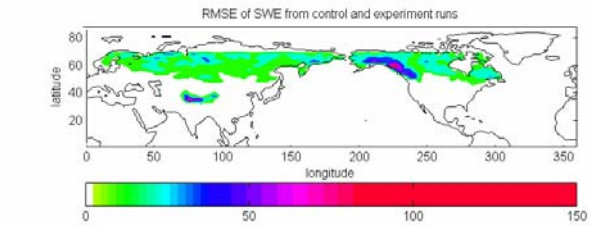

Figure2. Spatial distribution of RMSE of SWE from control and experimental runs

This work has been supported by the INTAS Project 03-51-5296 and NATO ESP CLG grant 981942.

References:

Brown, R. D., B. Brasnett and D. Robinson, 2003: Gridded North American Monthly Snow Depth and Snow Water Equivalent for GCM Evaluation, *Atmosphere-Ocean*, 41 (1), 1–14

Frei, A., R. Brown, J.A. Miller and D.A.Robinson, 2005, Snow mass over North America: observations and results from the second phase of the Atmospheric Model Intercomparison Project (AMIP-2), *Journal of Hydrometeorology*, 6, 681-695.

Khan V.M., K.G. Rubinshtein, A.B. Shmakin, 2007, Comparison of Seasonal and Interannual Variability of Snow Cover in Russian Watersheds According to Observations and Reanalyses , *Izvestiya, Atmospheric and Oceanic Physics*, Vol. 43, No. 1, pp. 69-80

Hall, A., and X. Qu (2006), Using the current seasonal cycle to constrain snow albedo feedback in future climate change, Geophys. Res. Lett., 33, L03502, doi:10.1029/2005GL025127.

Roesch, A., 2006, Evaluation of surface albedo and snow cover in AR4 coupled climate models, J. Geophys. Res., 111, D15111, doi:10.1029/2005JD006473

Sturm, M., J. Holmgren, G.E. Liston, A seasonal snow cover classification system for local to global applications, *J. Climate*, *8*(5), 1261–1283, 1995

Changes of seasonal ice area in the Arctic Ocean from model simulations with IPCC SRES scenario

V.Ch. Khon[1], I.I. Mokhov[1], E. Roeckner[2]

[1]A.M. Obukhov Institute of Atmospheric Physics RAS, Moscow, Russia
[2]Max-Planck Institute for Meteorology, Hamburg, Germany
(khon@ifaran.ru)

Analysis of sea ice characteristics such as a thickness and area of seasonal sea ice (or first-year ice) area was performed using simulations with global climate model ECHAM5/MPI-OM (Marsland et al., 2003; Roeckner et al., 2003) with the SRES A1B scenario (Houghton et al., 2001). This scenario reaches 720ppm CO2 levels by 2100 and is one of the middle SRES scenarios used in IPCC runs.

Sea ice concentration and thickness were used for calculating of seasonal sea ice area. Multiyear ice is ice that has survived at least one summer melt season (Zhang and Walsh, 2006). Consequently, we can use the summer minimum sea ice area as an indicator of multiyear ice area. Therefore we define an area of seasonal sea ice as the difference between the largest (April-May) sea ice area and the summer minimum (August-September) sea ice area (Holland et al., 2006) for each year. Sea ice thickness was averaged for areas with ice concentration more than 0.15. The Arctic region (68-90N) has been partitioned to the western (90W; 90E) and eastern (90E; 270E) parts for the regional analysis (ACIA, 2004).

Figure 1 shows March ice thickness (a) and the area of seasonal ice (b) as a function of the March ice thickness for the eastern and western parts of the Arctic basin. Over the run (Figure 1), the ice cover thins from about 2 m to less than 1 m for the western Arctic and from about 4 m to less than 1.5 m for the eastern Arctic. As a result there is increasing of seasonal ice area in the both regions. The strongest (nonlinearly as function of March ice thickness) increase of seasonal ice has been indicated for the eastern Arctic. For the western Arctic model results show weaker increasing of seasonal ice area with decreasing of ice thickness.

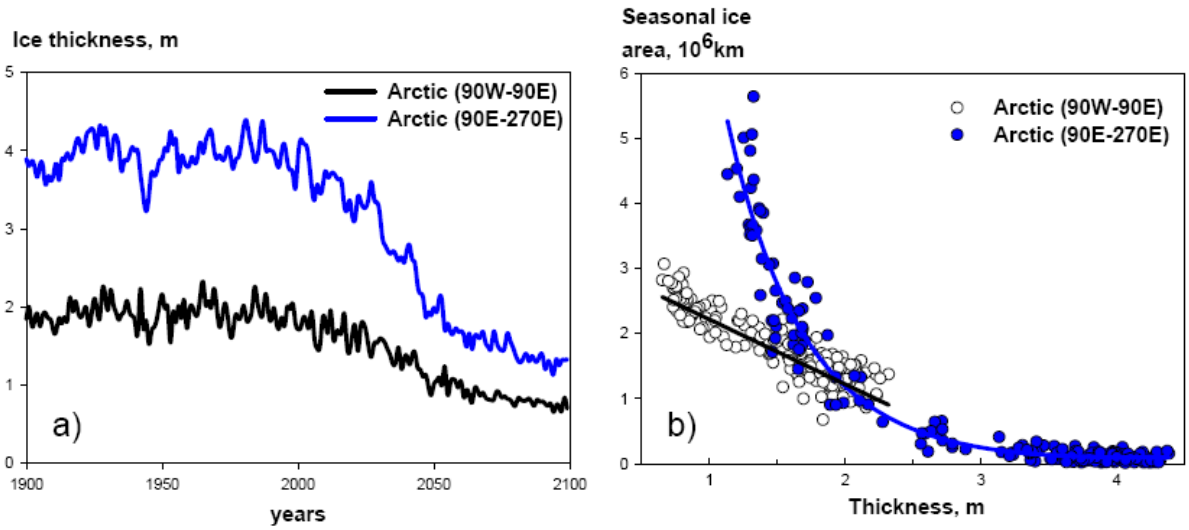

Figure 1. (a) March ice thickness and (b) the seasonal ice area as a function of the March ice thickness for the eastern and western parts of the Arctic basin. The seasonal ice area (or open water formation during melt season) equals the difference between the largest sea ice area and summer minimum sea ice area for each year.

This effect can be explained by changes in annual cycle of open water formation for the selected regions of the western (Barents Sea sector) and eastern (Laptev Sea sector) Arctic. Figure 2 shows mean area (in %) of open water in the sector of the Barents (a) and Laptev (b) Seas for the consequent 20-years periods (2001-2020, 2021-2040, 2041-2060, 2061-2080, 2081-2100) of model simulations. For the Barents Sea model results show nearly uniform increase of ice melting for each month. For the Laptev Sea there is strong increase of amplitude (difference between maximum and minimum ice extent) of annual cycle due to strong decrease of sea ice during melt season.

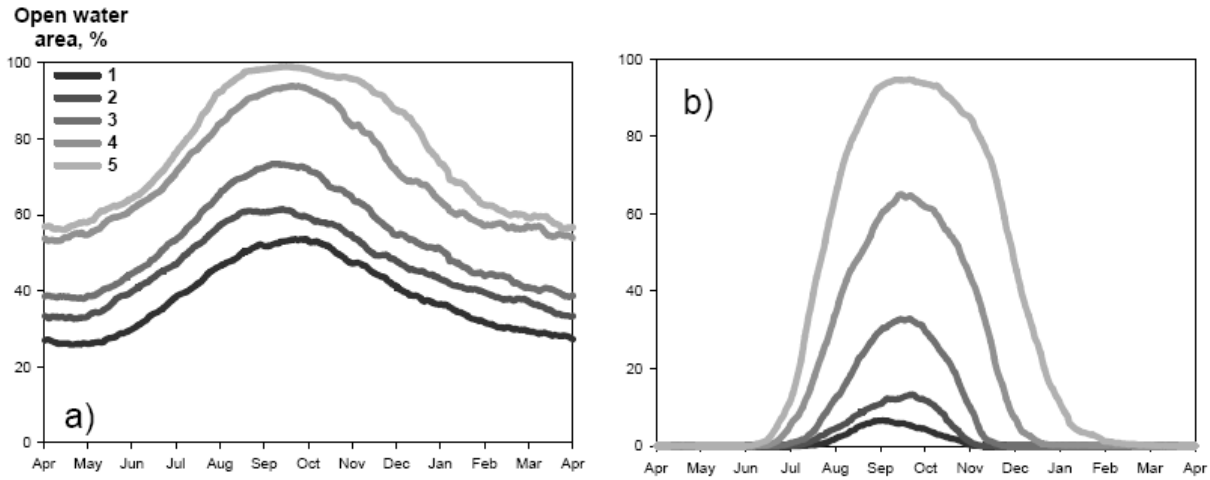

Figure 2. Open water area (%) in the Barents (a) and Laptev (b) Sea sectors according to model simulations for the consequent 20-years periods (1 – [2001-2020], 2 – [2021-2040], 3 – [2041-2060], 4 – [2061-2080], 5 – [2081-2100]).

According to model results an increasing of the open water area in the Barents Sea is connected with earlier ice melting and later ice freezing in the XXI century. For the Laptev Sea model results show the increase for intensity of ice melting (due to strong increasing of seasonal ice area) during warm season with a tendency to later ice freezing in the XXI century.

This work was supported by the Russian Foundation for Basic Research and INTAS Fellowship Grant for Young Scientists (06-1000014-6556).

References

Houghton, J. T., Y. Ding, D. J. Griggs, M. Noguer, P. J. van der Linden, X. Dai, K. Maskell, and C. A. Johnson, Eds., 2001: Climate Change 2001: The Scientific Basis. Cambridge University Press, 881 pp.

ACIA, 2004: Arctic Climate Impact Assessment: Scientific Report. Cambridge University Press, 144 pp.

Marsland, S. J., H. Haak, J. H. Jungclaus, M. Latif, and F. Röske, 2003: The Max-Planck-Institute global ocean/sea ice model with orthogonal curvilinear coordinates. Ocean Model., 5, 91–127.

Roeckner E., Bäuml G., Bonaventura L., Brokopf R., Esch M., Giorgetta M., Hagemann S., Kirchner I., Kornblueh L., Manzini E., Rhodin A., Schlese U., Schulzweida U., Tompkins A. The atmospheric general circulation model ECHAM 5. Part I: Model description / MPI Rep. 349, Max Planck Institute for Meteorology, Hamburg. 2003.

Zhang, X., and J. E. Walsh (2006), Toward a seasonally ice-covered Arctic Ocean: Scenarios from the IPCC AR4 model simulations, J. Clim., 19, 1730– 1747.

Holland, M. M., C. M. Bitz, and B. Tremblay (2006), Future abrupt reductions in the summer Arctic sea ice, Geophys. Res. Lett., 33, L23503, doi:10.1029/2006GL028024.

Impact of the North Atlantic thermohaline circulation on the European and Northern Atlantic weather in a coupled GCM simulation

V.Ch. Khon[1], M. Latif[2], I.I. Mokhov[1], E. Roeckner[3], V. A. Semenov[1,2]

[1]A.M. Obukhov Institute of Atmospheric Physics RAS, Moscow, Russia
[2]Leibniz Institute of Marine Sciences at the University of Kiel, Germany
[3]Max-Planck Institute for Meteorology, Hamburg, Germany
(khon@ifaran.ru)

Impact of the North Atlantic thermohaline circulation (THC) on the European weather characteristics has been analyzed using a 500-years control simulation with the global coupled atmosphere-ocean general circulation model ECHAM5/MPI-OM (Marsland et al., 2003; Roeckner et al., 2003) of spatial resolution T42 (Jungclaus et al., 2004; 2007; Pohlmann et al., 2006). Index of North Atlantic THC was defined as a maximum strength of ocean meridional overturning at 30N.

Correlations between annual mean North Atlantic THC index and precipitation, sea level pressure (SLP), and surface air temperature (SAT) has been computed for different seasons. The strongest correlations are found for boreal winter season, whilst summer season in general does not show significant correlations. The winter correlations are shown in the Figure 1.

As can be seen, the positive phase of the THC is related to increase of precipitation (decrease of SLP) over Norwegian-Barents Seas and northern Eurasia and warming over North Atlantic, Europe and northern Asia. These changes are due to increased sea surface temperatures (SST) in the Northern Atlantic related to the positive THC phase (Latif et al., 2004). These induce intensified advection from the ocean to the western part of Eurasia. Another mechanism is an increase of the oceanic inflow to the marginal Arctic seas with corresponding sea ice retreat. This causes particular strong correlations in the Norwegian and Barents Sea areas.

Changes in the SST can affect large-scale atmospheric circulation in the Northern Atlantic. Figure 2 shows 20-years running mean time series of annual North Atlantic THC index and anomalies of wintertime Icelandic Low intensity index in the control run.

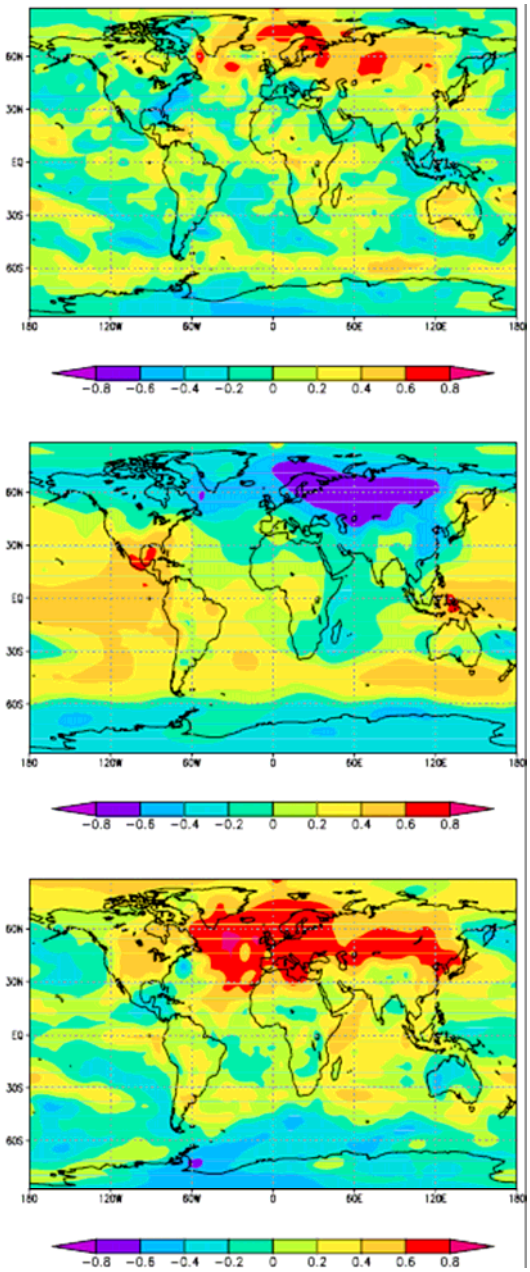

Figure 1. Correlations between low-passed (20-year running means) annual mean THC index and precipitation (top), sea level pressure (middle), surface air temperature (bottom) for the winter according to model simulations. 95% significance level is +- 0.45.

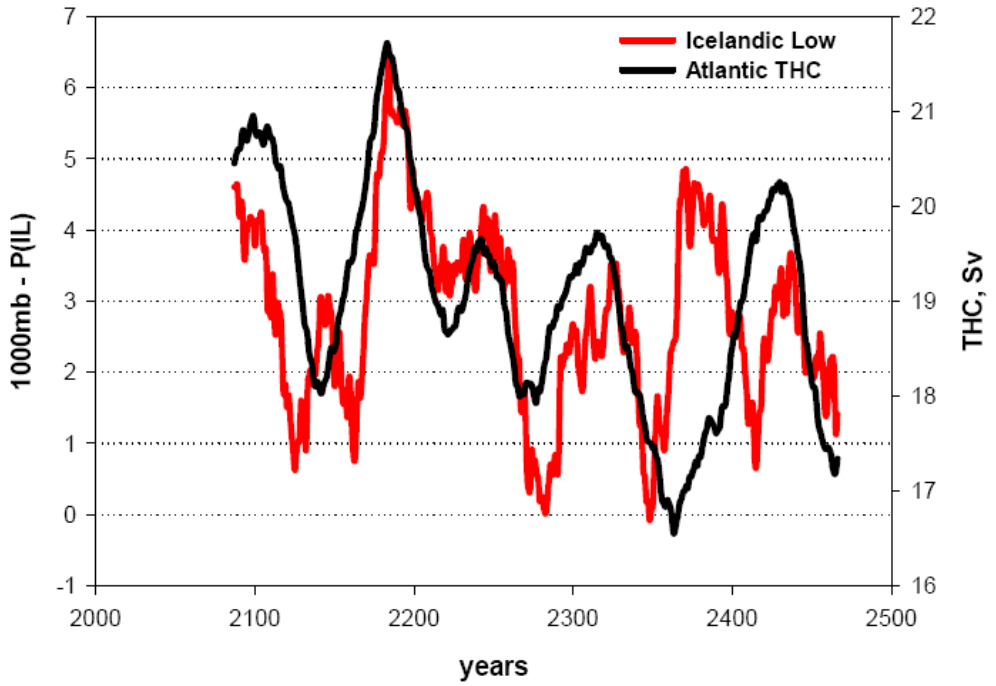

Figure 2 Time series of annual mean North Atlantic THC index and wintertime Icelandic Low (IL) intensity index (1000mb minus SLP in the center of IL) in the control run (20-years running means).

According to the model simulation (Figure 2), there is significant modulation of the Iceland Low intensity by the North Atlantic THC on the multidecadal timescale. Intensification of the Iceland Low (and increase of atmospheric zonal circulation, respectively) can produce large-scale positive anomalies in the surface air temperature over the Eurasian continent (Figure 1, bottom).

This work was supported by the Russian Foundation for Basic Research, NATO CLG grant 982423 (Collaborative Linkage Grant) and INTAS Fellowship Grant for Young Scientists (06-1000014-6556).

References

Jungclaus J., Haak H., Latif M., and U. Mikolajewicz (2005), Arctic-North Atlantic interactions and multidecadal variability of the meridional overturning circulation. J. Climate, 18, 4013-4031.

Latif, M., Roeckner, E., Botzet, M., Esch, M., Haak, H., Hagemann, S., Jungclaus, J., Legutke, S., Marsland, S., Mikolajewicz, U., and J. Mitchell (2004), Reconstructing, monitoring, and predicting multidecadal-scale changes in the North Atlantic thermohaline circulation with sea surface temperature. J. Climate, 17, 1605-1614.

Marsland, S. J., H. Haak, J. H. Jungclaus, M. Latif, and F. Rцske (2003) The Max-Planck-Institute global ocean/sea ice model with orthogonal curvilinear coordinates. Ocean Model., 5, 91–127.

Roeckner E., Bäuml G., Bonaventura L., Brokopf R., Esch M., Giorgetta M., Hagemann S., Kirchner I., Kornblueh L., Manzini E., Rhodin A., Schlese U., Schulzweida U., Tompkins A. The atmospheric general circulation model ECHAM 5. Part I: Model description / MPI Rep. 349, Max Planck Institute for Meteorology, Hamburg. 2003.

Pohlmann H., Sienz F., and M. Latif (2006), Influence of the multidecadal Atlantic meridional overturning circulation variability on European climate. J. Climate, 19, 6062-6067.

The transferability of Regional Climate Models through an assessment of the diurnal cycle

Zavareh Kothavala[1], Colin Jones[1], Dominique Paquin[2] and Ayrton Zadra[3]

[1] *Centre ESCER, Université du Québec à Montréal, Canada. (Email:* zav@sca.uqam.ca)
[2] *Ouranos Consortium, 550 Sherbrooke Street West, Montréal, Canada*
[3] *Recherche en Prévision Numérique, Meteorological Services of Canada, Dorval, Canada*

1. Introduction

Three Regional Climate Models (RCMs) were implemented over seven different regions of the globe with the objective of assessing their *transferability* to different climate regimes. This can be explained as the ability of RCMs to simulate the variability of continental scale climates over different regions of the world with minimal parameter changes [4]. The models are: the Rossby Centre Regional Atmospheric Climate Model (RCA3) from Sweden [3]; the Canadian Regional Climate Model (MRCC) [1]; and the climate version of the operational forecast model of Environment Canada (GEM) [2]. The RCMs were piloted by ERA-40 and NCEP boundary conditions for a five year period spanning from 2000 to 2004. To fully assess the ability of the RCMs to represent the observed variability, field observations collected as part of the Coordinated Enhanced Observation Period (CEOP) program over the same period, were used as a baseline. The variability of surface temperature, precipitation, humidity, wind speed, sensible heat, latent heat, and the surface radiation fields were examined. A succinct description of the analysis of the diurnal cycle of precipitation and temperature with three RCMs is presented for a site at a non-native domain spanning July to September 2001.

2. Analyses

Table 1 lists the observed average temperature and the difference from this value that was simulated by the RCA3, GEM, and MRCC models. In order to highlight the scope of the project, values from five sites in five different model domains are presented. These sites highlight different climate regimes and a different land surface characteristics. The Cabauw and Mongolia sites are grasslands situated in maritime and continental climates respectively. The BERMS site is over the boreal forest with Old Black Spruce vegetation. The Rondonia site covers a tropical rain forest in the Amazon. The site at Manus, is located on an island in the tropical western Pacific ocean.

For simplicity, one could regard an anomaly value close to ± 1 K to signify that the model simulations are similar to the observations. By this measure, RCA3 simulates temperature closest to the observations for four of the five sites in Table 1. GEM simulates temperature closest to the observed at Manus in the tropical western Pacific and is furthest from the observed at the BERMS boreal forest site. MRCC is closest to the observed over the tropical rain forest and is furthest from the observed over the boreal Black Spruce forest. To explain these differences, an examination of the diurnal cycle helps yield insight into the underlying model variability.

Site	lon	lat	CEOP Obs (K)	Model - Obs RCA3 GEM MRCC
1	4.93	51.97	289.94	-0.08, 1.69, -1.19
2	-105.1	53.99	289.77	-1.11, 2.11, -3.17
3	106.26	45.74	291.76	-0.75, -1.10, 2.73
4	-61.93	-10.08	299.01	4.17, 2.00, -0.93
5	147.43	-2.06	300.69	0.23, 0.19, -1.21

Table 1: Average July August and September 2001 2-meter temperature: 1. Cabauw; 2. BERMS Old Black Spruce; 3. Mongolia; 4. Rondonia; 5. Tropical Western Pacific (Manus). Negative anomaly values imply that the model is colder than observations.

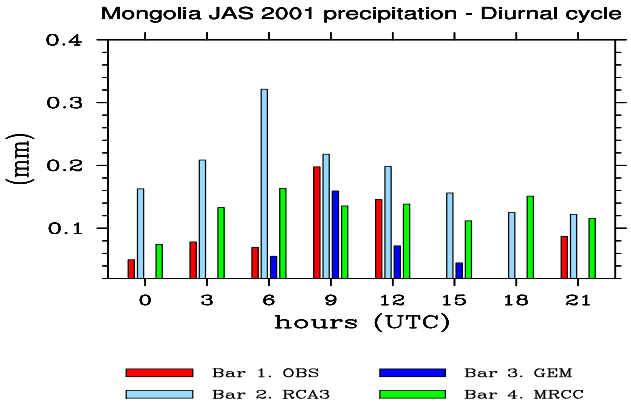

Figure 1: Diurnal cycle of JAS 2001 precipitation.

Figure 1 shows the diurnal cycle of precipitation of the three RCMs compared to the observations for Mongolia (local time = UTC + 8 hours). The precipitation accumulated over three-hour intervals were averaged over the 92 days from July to September 2001. The site experiences a dry continental climate. The CEOP observations show that the time of the day with the maximum precipitation is at 9 hours UTC. This implies that during the northern hemisphere summer, the site received most of

the daily precipitation in the late afternoon. The three RCMs simulate precipitation at night, unlike the observations. RCA3 simulates more than twice the total amount of precipitation observed during this period at this site, while GEM simulates less than half the amount observed.

Figure 2 shows the box-whisker diagrams of 3-hourly surface temperature for the observations and the RCMs at the same site and for the same period. The box shows the inter-quartile range and the whiskers show the 5% and 95% values. The CEOP observations show the maximum temperature of the day at 9 hours UTC (1700 hours local). This corresponds to the time of maximum precipitation in the afternoon. On the other hand, the three RCMs show the maximum temperature at 6 hours UTC. The excessive warm temperatures simulated by GEM causes greater dryness due to evaporation and subsequently the least precipitation. Interestingly, although RCA3 has an average temperature close to the CEOP observations, the range of temperatures is larger at all hours of the diurnal cycle. MRCC has the coldest temperatures at 18 and 21 hours UTC i.e. the early hours of the morning at this site.

3. Summary

Only two variables at one reference site and one season are examined here due to space limitations. It should be stressed that transferability is not an inter-comparison exercise. The understanding of the response of RCMs to different continental forcings have profound implications for the hydrologic cycle and associated feedbacks, which are vital to the study of present and future climates. The analyses of these processes are currently being assessed.

References

[1] D. Caya and R. Laprise. A semi-implicit semi-Lagrangian regional climate model: The Canadian RCM. *Monthly Weather Review*, 127:341–362, 1999.

[2] J. Côté, S. Gravel, A. Methot, A. Patoine, M. Roch, and A. Staniforth. The operational CMC-MRB Global Environmental Multiscale (GEM) model. Part I: Design considerations and formulation. *Monthly Weather Review*, 126:1373–1395, 1998.

[3] C.G. Jones, U. Willen, A. Ullerstig, and U. Hansson. The Rossby Centre regional atmospheric climate model Part 1: Model climatology and performance for the present climate over Europe. *Ambio*, 33:199–210, 2004.

[4] E.S. Tackle, J. Roads, B. Rockel, W.J. Gutowski Jr, R.W. Arritt, I. Meinke, C.G. Jones, and A. Zadra. Transferability Intercomparison: An opportunity for new insight on the global water cycle and energy budget. *Bulletin of the American Meteorological Society*, 88:In Press, 2007.

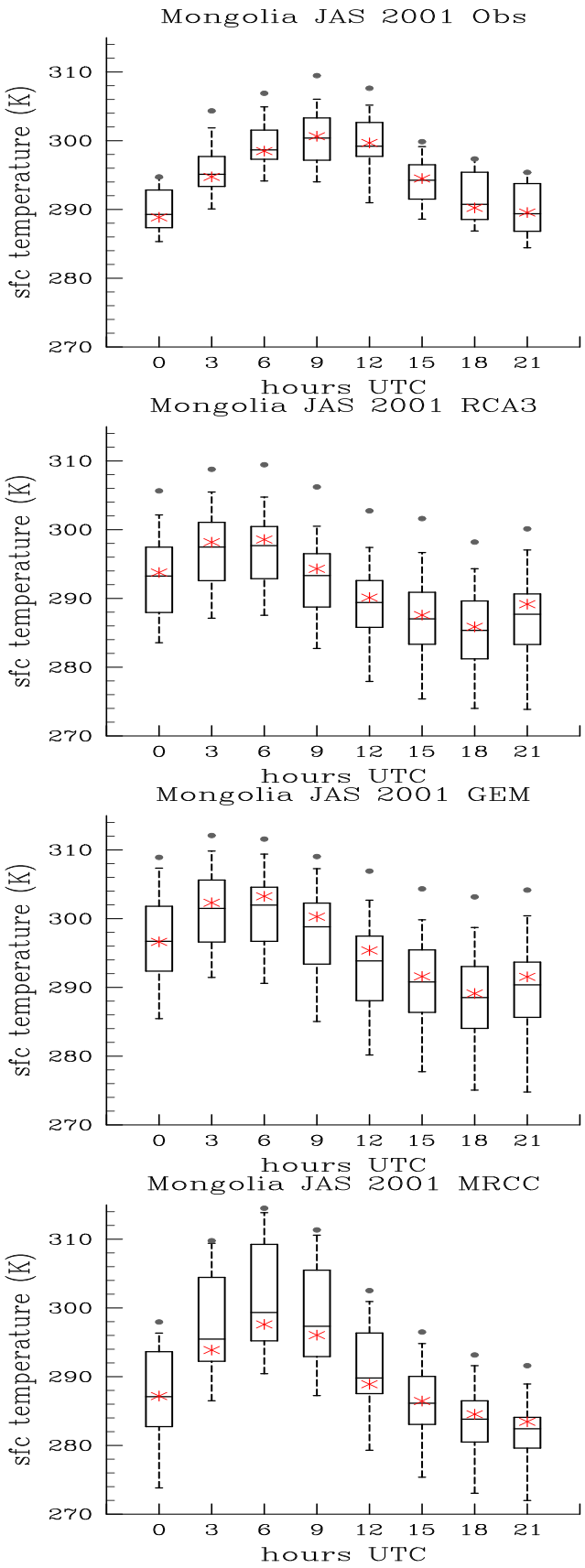

Figure 2: Box-whisker diagrams of 3-hourly surface temperature during July to September 2001 (⋆=mean).

Sensitivity of the general circulation and extratropical cyclone characteristics to tropical and polar heating

Eun-Pa Lim[1] and Ian Simmonds[2]

[1]Bureau of Meteorology Research Centre, GPO Box 1289K, Victoria 3001, Australia
[2] School of Earth Sciences, University of Melbourne, Victoria 3010, Australia
E-mail: e.lim@bom.gov.au

In a warmer globe caused by increasing CO_2 greater warming is expected over the polar region in the lower troposphere and over the tropics in the upper troposphere (Figure 1) (IPCC 2001), and Southern Hemisphere winter extratropical cyclones in the CSIRO Mark2 atmosphere-ocean coupled model are seen to reduce in their number with doubled CO_2 (Figure 2) (Sinclair and Watterson 1999, Lim 2005). In this study we examine the influence of each of the tropical and the polar warming on the general circulation and the characteristics of Southern Hemisphere (SH) extratropical low pressure systems by conducting idealised temperature 'nudging' experiments.

Using Melbourne University atmospheric general circulation model (MUGCM, R21/L9), warm temperature anomaly, 0.04ºC hr^{-1} was nudged over (a) the tropics between 21.5ºS and 21.5ºN at sigma level = 0.336 - TU (Tropics/Upper level); (b) the high latitudes between 65ºand 90º latitudes in both hemispheres at sigma = 0.991 and 0.926 - HL (High latitude/Lower level); and (c) the tropics at sigma = 0.336 and the high latitudes at sigma = 0.991 and 0.926 - TU+HL. These warm anomalies were forced at all points on the relevant latitude circles. The resultant vertical temperature profile is shown in Figure 3.

Our three sets of 8 year MUGCM simulations demonstrate that warming over the tropics in the upper troposphere results in stronger Ferrel circulation and westerlies between 40ºS and 60ºS in winter. Whereas, warming over the high latitudes in the lower troposphere causes the meridional and vertical circulations to be slightly weaker over most of the SH extratropics and the upper level zonal winds to be less strong over the 60ºS latitude band. When the equal amount of positive temperature anomaly was nudged over the high latitudes in the lower troposphere and over the tropics in the upper troposphere, the weakening of the meridional-vertical circulation is more obvious than that in the HL experiment. The axis of westerly jet tends to move equatorward.

Figure 4 shows zonal means of winter MSLP cyclone system density and depth which were simulated in three different nudging experiments. Warming in the TU experiment tends to cause the frequency and depth of extratropical cyclones to increase in the high latitudes at the surface. By contrast, warming over the high latitudes in the lower troposphere (HL and TU+HL), the frequency and depth of MSLP cyclones tend to decrease in the higher latitudes. In the midlatitudes between 30º-50ºS fewer surface cyclones are found with the TU warming, but slightly more systems are found with the HL and TU+HL warming. However, the cyclone property changes with the HL and TU+HL warmings are very subtle in the midlatitudes, and it needs further investigation whether this less sensitivity to the polar warming is model dependent or not.

Consequently, the TU warming seems an important contributor to the decrease in cyclone system density over most of the SH extratropics in a doubled CO_2 atmosphere shown in Figure 2.

IPCC (2001). Climate Change 2001, The scientific basis, edited by Houghton, J. T., Y. Ding, D. J. Griggs, M. Noguer, P. J. van der Linden, X.Dai, K. Maskell and C. A. Johnson. Cambridge, U.K.: New York, USA: Cambridge University Press.

Lim, E.-P. (2005). Global changes in synoptic activity with increasing atmospheric CO_2, Ph. D. thesis, University of Melbourne, Victoria, Australia

Sinclair, M. R. and I. G. Watterson (1999). Objective assessment of extratropical weather systems in simulated climates, *Journal of Climate*, **12**, 3467-3485.

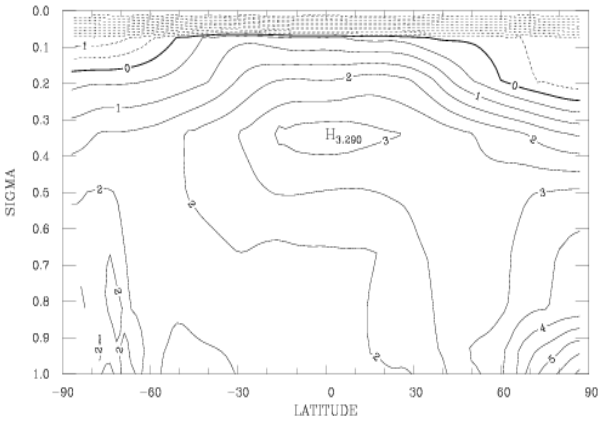

Figure 1 Vertical profile of annual mean temperature change of 2xCO2-1xCO2 simulated in the CSIRO Mk2 AOGCM. The contour interval is 0.5 K.

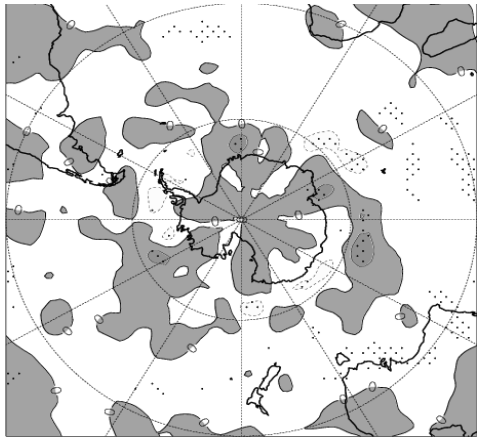

Figure 2 Changes in MSLP cyclone system density from 1xCO2 to 2xCO2 simulated in the CSIRO Mk2 AOGCM. Shaded areas show positive changes, and stiples show statistically significant changes at the 95% confidence level

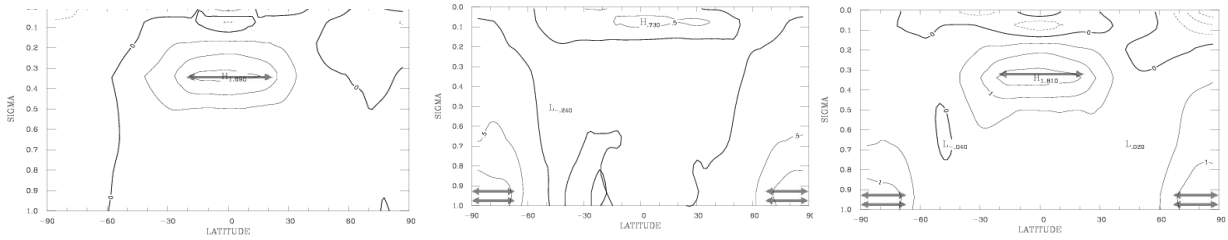

(a) (b) (c)

Figure 3 Vertical profile of annually averaged temperature difference between the control experiment and (a) the tropical/upper troposphere (TU) warming, (b) the high latitudes/lower troposphere (HL) warming, and (c) the TU+HL warming experiments. The arrows indicate the locations where the temperature forcing is placed. The contour interval is 0.5 K.

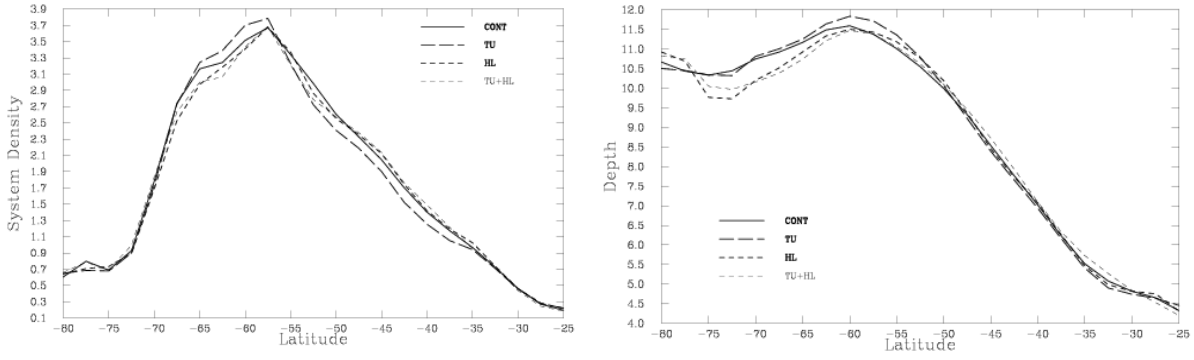

(a) (b)

Figure 4 Zonal means of MSLP cyclone (a) system density and (b) depth simulated in the control run (solid line) and the transient runs with the TU warming (solid long dash line), the HL warming (solid short dash line), and the TU+HL warming (short dash line)

Categorical predictability of regionalized surface temperature and precipitation over the southeast United States

Young-Kwon Lim, D. W. Shin, T. E. LaRow, and S. Cocke
Center for Ocean-Atmospheric Prediction Studies, Florida State University, Tallahassee, FL 32306-2840
(lim@coaps.fsu.edu)

Coarsely resolved surface temperature and precipitation which are seasonally integrated using the FSU/COAPS GSM (Florida State University/Center for Ocean-Atmospheric Prediction Studies Global Spectral Model, ~1.8° lon.-lat. (T63)) for the period of 1994 to 2002 (March through September each year) are downscaled to local spatial scale of ~20 km for the southeast United States (Florida, Georgia, and Alabama) by applying both dynamical and statistical methods. This study is performed since 1) the individual local areas over the southeast United States frequently face extremely high temperature and the heavy rainfall with severe storms during summer, resulting in the devastating property damage and injuries. An accurate seasonal forecast with higher spatial resolution is essential to mitigate damage in advance. 2) This region is also noted for some of the largest areas of agricultural farms in the nation. Various kinds of crops and fruits (e.g., peach, tomato, corn, tangerine, peanut, citrus, and strawberry) are raised in these regions. Farmers and agricultural researchers need accurate climate forecasting to adapt management, increase profits, and reduce production risks.

Dynamical downscaling is conducted by running the FSU/COAPS Nested Regional Spectral Model (NRSM), which is nested into the domain of the FSU/COAPS GSM (GSM) (Shin et al. 2006; Cocke et al. 2007). A statistical downscaling is newly developed in this study. The rationale for this approach is that clearer separation of prominent local climate signals (e.g., seasonal cycle, dominant intraseasonal or interannual oscillations) in the observations and the GSM over the training period can facilitate the identification of the statistical relationship associated with climate variability between two datasets, which eventually leads to better prediction of local climate scenario from the large-scale simulations. The techniques primarily applied for statistical downscaling are Cyclostationary EOF (CSEOF) [*Kim and North*, 1997], multiple regressions, stochastic time series generation, and the cross-validation. Overall downscaling procedures are illustrated by the schematic diagram in Fig. 1.

Downscaled data are compared with the FSU/COAPS GSM fields and observations. Downscaled seasonal anomalies reasonably produce the local surface temperature and precipitation scenario from the coarsely resolved large-scale simulations. A series of evaluations including correlations, frequency of extreme events, and categorical predictability demonstrate the reliability of these downscaling models. As shown in Fig. 2 and 3 as examples, categorical predictability for seasonal maximum temperature anomaly (T_{max}) and rainy/dry periods reveals the correctness in percentage prevailing from 60 to 80 (T_{max}) and, from 50 to 70 (precipitation) by both downscaling methods, supporting that our downscalings yield the predictability perceptibly greater than random chance. The skill of this local forecast is comparable to or greater than predictability of large-scale NCEP climate seasonal forecasts [*Saha et al*., 2006]. Much lower incorrectness in percentage shown on the second and third column of figures, and the Heidke skill scores on the fourth column demonstrate the reliable skill of these downscaling approaches. Although there still remains a room for the improvement in predictive skill, these downscaled model results are reliable and can be used in many application models (e.g., crop model).

Acknowledgement
COAPS receives its base support from the Applied Research Center, funded by NOAA Office of Global Programs awarded to Dr. James J. O'Brien.

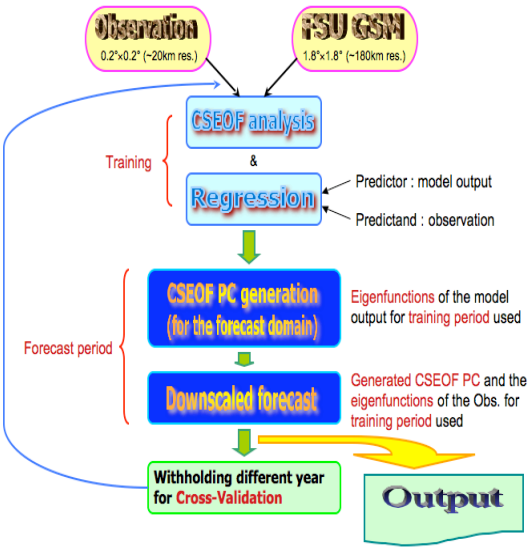

Figure 1. Schematic diagram of statistical downscaling procedure in the present study. Downscaling has been conducted using Cyclostationary EOF, multiple regression, and the time series generation techniques. Downscaled data are produced over 9 years (1994-2002) by repeatedly withholding a particular year and placing it on the prediction period under the cross-validation framwork.

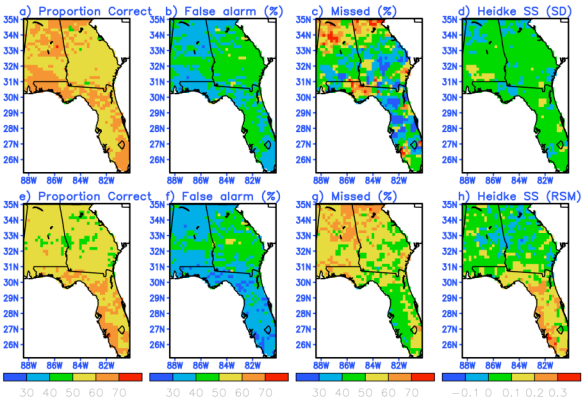

Figure 3. Same as Fig. 2 but for rainfall periods. The 5-day interval during which precipitation amount is greater than 5mm is classified into wet period otherwise the dry period (see table right).

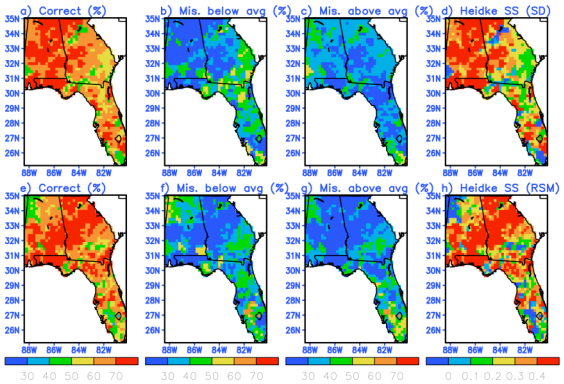

Figure 2. Categorical predictability in percentage (the left three columns) and Heidke Skill Score (right column) for the downscaled seasonal T_{max} anomaly. Two classes from categorization are 1) above climatological T_{max} and 2) below climatological T_{max}. Top panel depicts the result from the statistical downscaling whereas bottom panel the dynamical downscaling (the NRSM). The first three columns from the left illustrate the percentage of 1) correct prediction (the sign of downscaled anomaly & observed anomaly is same), 2) $\frac{P_{ab}}{P_{aa}+P_{ab}}\times 100$ (see the schematic probability table below), and 3) $\frac{P_{ba}}{P_{ba}+P_{bb}}\times 100$ (see table below).

Verifying analysis		Downscaled Forecast: above average	Downscaled Forecast: below average	
Obs.	Above	P_{aa}	P_{ba}	P_a^P
	Below	P_{ab}	P_{bb}	P_b^P
		P_a^F	P_b^F	1

Verifying analysis		Downscaled Forecast: wet period	Downscaled Forecast: dry period	
Obs.	wet period	P_{aa}	P_{ba}	P_a^P
	dry period	P_{ab}	P_{bb}	P_b^P
		P_a^F	P_b^F	1

References

Cocke, S., T. E. LaRow, and D. W. Shin, 2007: Seasonal rainfall prediction over the southeast U.S. using the FSU nested regional spectral model. *J. Geophys. Res.*, **112**, D4, D04106, doi:10.1029/2006JD007535.

Saha, S., and Coauthors, 2006: The NCEP climate forecast system. *J. Climate*, **19**, 3483-3517.

Shin, D. W., J. G. Bellow, T. E. LaRow, S. Cocke, and J. J. O'Brien, 2006: The role of an advanced land model in seasonal dynamical downscaling for crop model application. *J. Appl. Meteor. Climatol.*, **45**, 686-701.

The Simulated Surface Radiation Budget over North America in a Suite of Regional Climate Models

Marko Markovic[1], Colin Jones[1], Paul Vaillancourt[2], Dominique Paquin[3]
[1]*University of Quebec at Montreal,* [2]*Environment Canada,* [3]*Consortium Ouranos*
markovic@sca.uqam.ca

Downward longwave radiation (DLR) and shortwave radiation (ISR) are important parameters in climate models, being the main terms in the surface energy balance controlling the evolution of surface temperature and soil moisture. Systematic biases in the representation of surface radiation can lead to errors in a number of key near surface climate variables (e.g. soil moisture, snow cover and sea-ice). In this report we evaluate the DLR and ISR simulated by 3 Regional Climate Models (RCMs) over North America. The RCMs used are: The Canadian Regional Climate Model (CRCM, version 4.0.2) (Caya and Laprise 1999), GEM-LAM, the regional version of the Global Environmental Multiscale Model (Côté et al 1998) and the Swedish Rossby Centre Regional Climate Model, RCA3, (Jones et al. 2004). Observations are derived from six measurement sites within the NOAA-SURFRAD (Surface Radiation Budget) network, representing a cross-section of various climate types over North America. 3-hourly, grid point DLR and ISR values, collocated with the 6 SURFRAD sites, were extracted from the respective RCM simulations and form the basis for an evaluation of the simulated surface radiation.

Figure 1 presents a normalized frequency distribution (FD) of surface ISR and DLR separately for summer (JJA) and winter (DJF) from the 3 models and surface observations. The FDs are averaged over the 6 observation sites. Cloud free conditions are defined as a given 3-hour period having a cloud cover less than 10% in both observations and model, while cloudy conditions are when each data set has a cloud cover value greater than 90%. All sky is the total surface radiation for all cloud cover conditions.

The DJF distribution of all-sky DLR (Fig. 1d) shows all models biased towards low values. For RCA3 and GEM-LAM this is due to a negative bias in the clear-sky DLR frequency distribution (Fig. 1e), cloudy-sky DJF DLR (Fig. 1f) being well simulated by these 2 models. A negative bias in simulated clear sky DLR in cold, dry winter conditions was also seen by Wild et al. (2000). This problem is often due to inaccuracies in either the representation of the water vapor continuum in dry conditions or deficiencies in including the contribution of trace gases and aerosols to the total DLR. CRCM has the same DLR clear-sky error (Fig. 1e) but also a negative bias in DJF DLR under cloudy skies (Fig. 1f). GEM-LAM and CRCM represent the distribution of all-sky DJF ISR well (Fig. 1a). Clear sky ISR DJF (Fig. 1b) is accurate in both models, while GEM shows the best result in cloudy conditions (Fig. 1c). The cloudy-sky DJF ISR is biased low in CRCM, suggesting winter clouds are optically too thick with respect to solar radiation. This is in contrast to the DJF DLR cloudy-sky errors in CRCM, biased towards low values, which is consistent with too low cloud emissivity. Cloud water appears to be treated in an inconsistent manner between the 2 radiation streams in CRCM. The negative bias in CRCM DJF cloudy-sky ISR (Fig. 1c) is balanced by an overestimate of the occurrence of clear-sky conditions (underestimated cloud cover, *not shown*). RCA3 DJF all sky ISR (Fig. 1a) has too few occurrences of low ISR ($< 200 Wm^{-2}$) and too many occurrences in the range $200\text{-}600 Wm^{-2}$. RCA3 simulated clouds in DJF appear to contain too little water or have a systematic underestimate in the effective radius leading to winter clouds that have too low albedo. Clear sky DJF ISR (Fig. 1b) is quite accurate in RCA3.

In JJA CRCM has a bias towards low values of all-sky DLR (Fig.1j), due to an underestimate of cloudy-sky DLR (Fig. 1l), also consistent with an underestimate of cloud emissivity. The negative bias in cloudy-sky DLR in CRCM during JJA is partially balanced by a positive bias in clear-sky DLR. This arises either from the CRCM atmosphere being too warm, and/or clear-sky conditions in CRCM, at high

water vapor concentrations, being frequently simulated as cloud-free while the same moisture conditions produce a cloud in observations (CRCM systematically underestimates JJA cloud cover, *not shown*). GEM-LAM has a similar bias to CRCM in clear sky JJA DLR (Fig. 1k), probably for similar reasons.

RCA3 gives an accurate JJA ISR all-sky distribution (Fig. 1g) while both GEM-LAM and CRCM overestimate the occurrence of high ISR values. RCA3 is biased towards too many occurrences of very low ISR (<200Wm^{-2}) in JJA cloudy conditions (Fig. 1i), consistent with summer clouds that are frequently optically too thick. This also helps explains the positive bias in the frequency of very high value cloudy-sky DLR (>440Wm^{-2}) in RCA3 in JJA(Fig. 1l). All 3 models underestimate cloud fraction in the JJA, we therefore conclude that the accurate total sky ISR (Fig. 1g) in RCA3 results from an overestimate of clear-sky radiation, due to an overestimate of clear-sky occurrence, balanced by clouds that are too reflective when present. GEM-LAM has numerous occurrences of very high cloudy-sky ISR in JJA (>800Wm^{-2}) (Fig. 1i). These cloudy-sky ISR values only occur for optically thin cirrus, suggesting an overestimate of these cloud types in GEM-LAM. The JJA ISR bias in CRCM seems mainly due to clear sky errors (e.g. the clear sky is too transmissive).

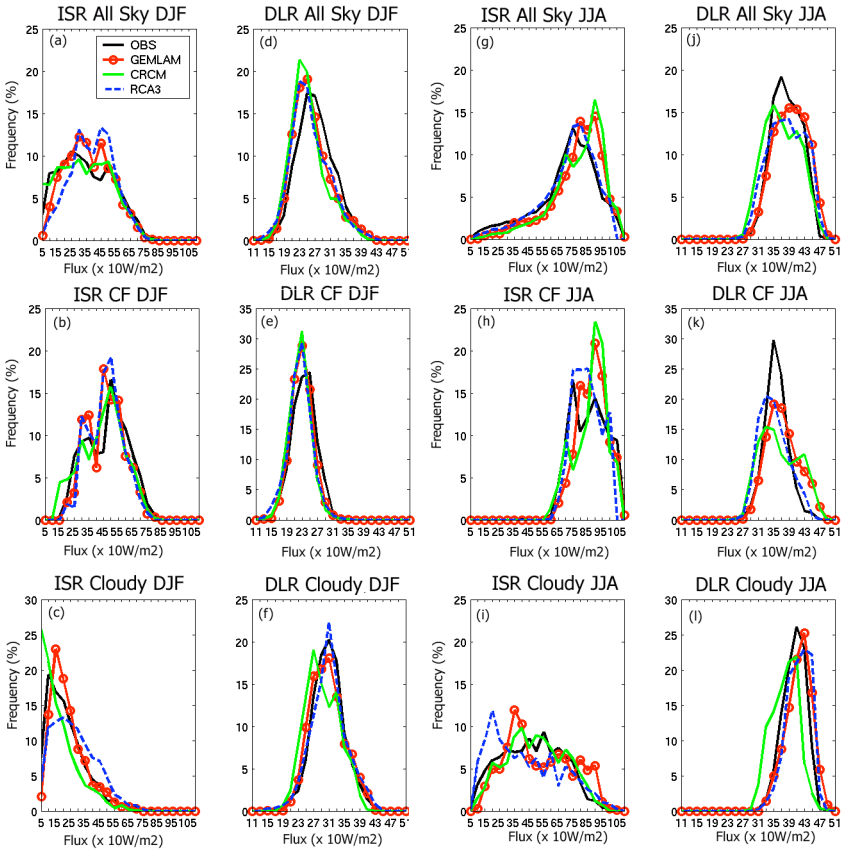

Figure 1: Distribution of ISR and DLR 3-hourly radiation fluxes from RCMs and observations. The period 15-21 UTC is analysed due to cloud observations only being available during sunlight: a) winter ISR all sky, b) winter ISR cloud free, c) winter ISR cloudy, d) winter DLR all sky, e) winter DLR cloud free, f) winter DLR cloudy, g) summer ISR all sky, h) summer ISR cloud free, i) summer ISR cloudy, j) summer DLR all sky, k) summer DLR cloud free, l) summer DLR cloudy.

References:

Caya D and Laprise R. 1999: A Semi-Implicit Semi-Lagrangian Regional Climate Model: The Canadian RCM. *Monthly Weather Review*, 127: 341-362.

Jones, C. G., Willén, U., Ullerstig, A. and Hansson, U 2004: The Rossby Centre Regional Atmospheric Climate Model Part I: Model Climatology and Performance for the Present Climate over Europe. *Ambio 33:4-5,* 199-210., 2004

Cote, J., S. Gravel, A.Methot, A. Patoine, M. Roch, and A. Staniforth 1998: The operational CMC-MRB global environmental multiscale (GEM) model. Part I: Design considerations and formulation. Mon. Wea. Rev, 126, 1373-1395.

Wild et al. Evaluation of Downward Longwave Radiation in General Circulation Models, Journal of Climate, 2000

Comparison of cloudiness and cyclonic activity changes over extratropical latitudes in Northern Hemisphere from model simulations and from satellite and reanalysis data

I.I. Mokhov[1], M.G. Akperov[1], A.V. Chernokulsky[1], J.-L. Dufresne[2], H. Le Treut[2]

[1]Obukhov Institute of Atmospheric Physics RAS, Moscow, Russia
[2]Laboratoire Meteorologie Dynamique du CNRS, Paris, France
mokhov@ifaran.ru

Changes of cloudiness and cyclonic activity over extratropical latitudes in the Northern Hemisphere (NH) from simulations with the coupled general circulation model (CGCM) are analyzed in comparison with satellite and reanalysis data.

Results of the IPSL-CM4 (version 1) CGCM (Marti et al., 2005) simulations for 1860-2000 with the greenhouse gases concentrations in the atmosphere from observations and for 2001-2100 with the SRES-A2 scenario are used.

Model results are compared to the cyclonic activity characteristics (Bardin and Polonsky, 2005; Golitsyn et al., 2006; Golitsyn et al., 2007) on the basis of NCEP/NCAR reanalysis data (Kistler et al., 2001) during 1952-2000 and to the satellite cloudiness data (Rossow and Duenas, 2004) for 1983-2000.

Daily data for cyclonic characteristics from model simulations were obtained similar to (Bardin and Polonsky, 2005; Golitsyn et al., 2006; Golitsyn et al., 2007). Here we analyze, in particular, the part of total area covered by cyclones or density of cyclones packing (DCP) defined similar to (Mokhov et al., 1992).

Figure 1 shows changes of total cloudiness and DCP over extratropical latitudes (20-80^{o}N) from model simulations for periods 1860-2000 (a) and 2001-2100 (b). Values on Fig.1 were normalized on their mean values for the period 1961-1990. Figure 1a does not show significant changes in total cloudiness and DCP while Fig.1b shows tendency of decrease for both variables in the 21st century. This tendency is related to a general tendency of decrease in the temperature difference between high and low latitudes with a general decrease of tropospheric baroclinic instability under global warming (Mokhov et al., 1992).

Analysis of relationship between total cloudiness by satellite monthly data and DCP by reanalysis monthly data for the NH extratopics shows significant positive correlation for the period 1983-2000 while no correlation was found by annual-mean data. Model simulations do not exhibit significant correlation for this period both by monthly-mean and annual-mean data but display positive correlation for longer periods during 1860-2100. Figure 2 shows relationship between total cloudiness and DCP for the NH extratopics from model simulations for the 21st century.

This work was supported by the CNRS/RAS Joint Agreement Program, Russian Foundation for Basic Research, Programs of the Russian Academy of Sciences and Russian President Scientific Grant.

References

Bardin, M.Yu., and A.B. Polonsky, 2005: North Atlantic Oscillation and synoptic variability in European-Atlantic region in winter period. *Izvestiya, Atmos. Oceanic Phys.*, **41**, 127-136.

Golitsyn, G.S., I.I. Mokhov, M.G. Akperov, and M.Yu. Bardin, 2006: Estimates of hydrometeorogical risks and dostribution functions for cyclones and anticyclones in dependence on their size and energy after reanalysis and some climate models. Intern. conf. on the problems of hydrometeorological security, Plenary's abstracts, Moscow, 35.

Golitsyn, G.S., I.I. Mokhov, M.G. Akperov, and M.Yu. Bardin, 2007: Probability distribution functions for cyclones and anticyclones. Doklady, Earth Sci. (in press)

Kistler, R., E. Kalnay, W. Collins. et al., 2001: The NCEP 50-year reanalysis: monthly means CD-ROM and documentation. *Bull. Amer. Met. Soc.*, **82**, 247-266.

Marti, O. et al., 2005. The new IPSL climate system model: IPSL-CM4**.** http://dods.ipsl.jussieu.fr/omamce/IPSLCM4/DocIPSLCM4/FILES/DocIPSLCM4.pdf

Mokhov, I.I., O.I. Mokhov, V.K. Petukhov, and R.R. Khairullin, 1992: Influence of global climate changes on eddy activity in the atmosphere. *Izvestiya, Atmos. Oceanic Phys.*, **28**, 11-26.

Rossow, W.B., and E. Duenas, 2004: The International Satellite Cloud Climatology Project (ISCCP) web site: An online resource for research. *Bull. Amer. Meteorol. Soc.*, **85**, 167-172.

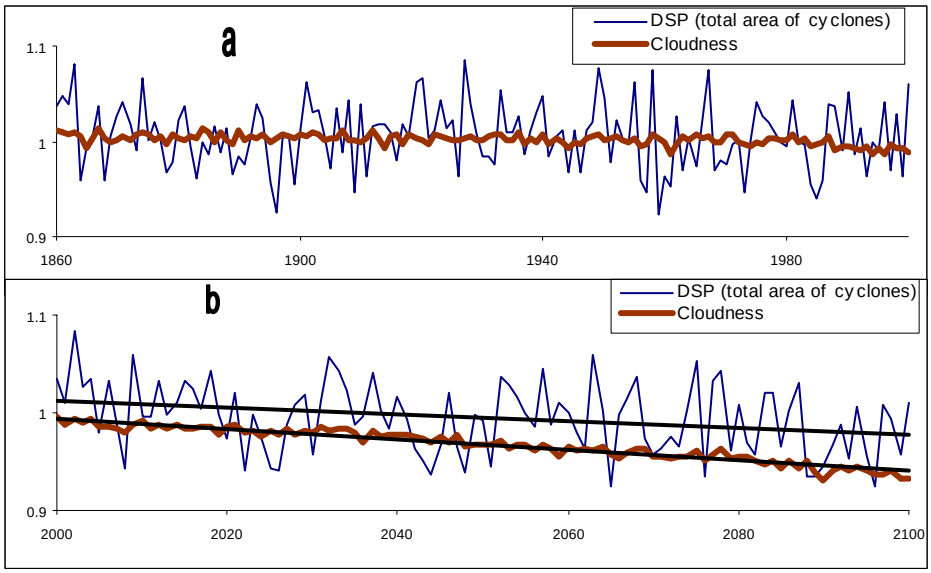

Fig. 1. Changes of normalized total cloudiness and DCP over extratropical latitudes (20-80N) from model simulations for periods 1860-2000 (a) and 2001-2100 (b).

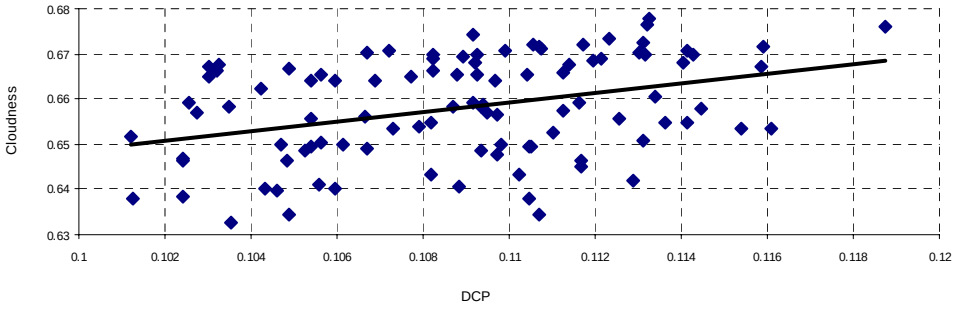

Fig. 2. Total cloudiness independence on DCP for the NH extratopics from model simulations for the 21st century.

Comparison of Cloud Microphysics between GEM and ARM-SGP Observations

Danahé Paquin-Ricard[1], Colin Jones[1], Paul Vaillancourt[2]
[1]CRCMD, Université du Québec à Montréal, [2]Environnement Canada
danahe@sca.uqam.ca

Introduction

Microphysical processes play a key role in controlling the liquid and ice water content of simulated clouds and, as a result, are important controls on precipitation and on the interaction of clouds with both solar and terrestrial radiation. Due to their extreme complexity most microphysical processes are highly parameterized in present-day climate models. In this article, we evaluate the microphysical parameterizations in the new Canadian Regional Climate Model, based on the limited area version of GEM (Global Environmental Multiscale Model, [1]). We compare simulated frequency distributions of Liquid Water Path (LWP) and precipitation rate, with observed distributions.

Model and Observations

Observations comes from the ARM Southern Great Plains (SGP) site, at the central facility (CF-1). Data streams used for this model evaluation are the "improved MicroWave Radiometer RETrivals of cloud liquid water (LWP) and precipitable water vapor (PWV)" (MWRRET, www.arm.gov/data/pi_products.stm) with LWP and PWV retrieved from the 2-channel microwave radiometer, the "Surface Meteorological Observation Station" (SMOS) which gives precipitation as a 1min average and the "ShortWave Flux Analysis on SIRS data by the LONG algorithm" (SWFANAL, [2]) which provides observed surface shortwave radiation and cloud cover at a 15min time resolution.

GEM uses a prognostic total cloud water variable, with a Sundqvist-type, bulk-microphysics scheme. GEM-LAM was integrated for the period 1998-2004 over a domain centred on the ARM-SGP site CF-1 (37°N, 97 °W). The integration used ECMWF reanalysis as lateral boundary conditions, prescribed SSTs and employed a horizontal resolution of ∼42km.

Both observations and model are averaged (for LWP) or accumulated (for precipitation) over 3h periods for the entire 7 years. The MWR cannot operate when its teflon window is wet. For this reason, all precipitation events greater than 0.25mm/3h are removed from the dataset of LWP for both observations and model. The uncertainty of observations is estimated to be around $\pm 15 g/m^2$ for LWP and ±0.25mm under normal conditions (without strong winds) for precipitation.

Results

In this section, we present results from one season, the winter (DJF), to focus on particularities of the winter cloud and synoptic regimes. We present normalized frequency distributions of LWP or precipitation for observations, in blue, and model, in red. The frequency of occurence of each bin represent a percentage of the observed or modelled total occurence separately. The first bin is divided by 10 due to its disproportionate size. Values on the x-axis represent a centred value for that bin.

Figure A shows the normalized PDF of LWP for observations and model. Relative to observations, GEM underestimates the occurence of LWP (for LWP$\geq 30 g/m^2$) and overestimates the occurence of LWP between 0 and $15 g/m^2$. This underestimate can arise from a number of sources such as: an overestimate of cloud-free occurences, precipitation too frequently triggered at too low LWP in the simulated clouds, or from an incorrect separation of cloud water into liquid and ice. If precipitation is triggered at too low LWP, there are two consequences: (i) the LWP value is removed from the model results and (ii) the simulated LWP is reduced due to precipitation removal.

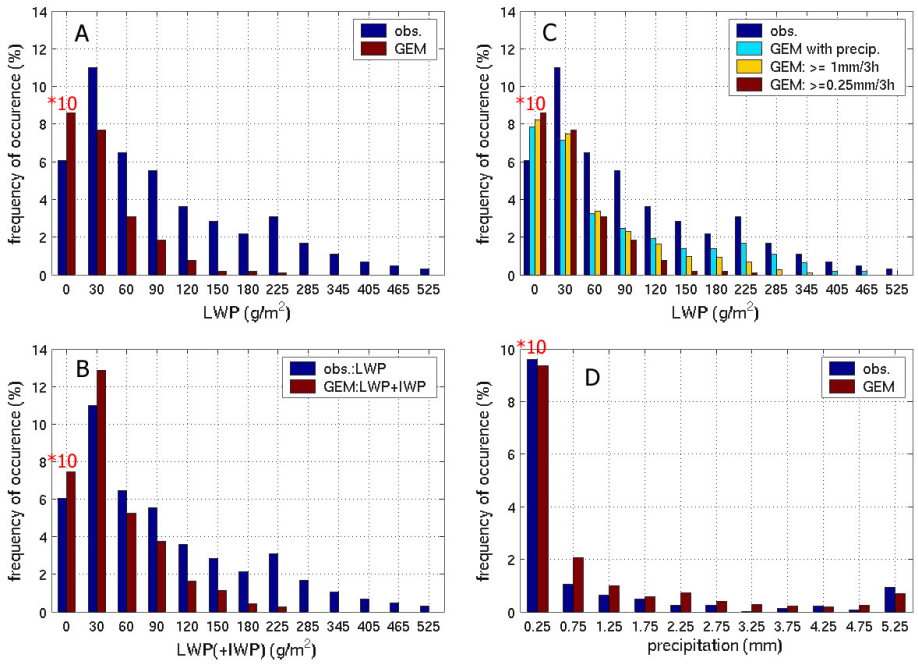

Figure B shows the same observations as in A, but, for the GEM results, the ice water path (IWP) is combined with LWP to determine whether some of the model LWP underestimate arises from the model classifying liquid as ice to frequently. Even with the inclusion of IWP, GEM still underestimate the occurence of high amounts of LWP ($\geq$90g/m^2). This underestimation occurs at a LWP range where cloud albedo varies greatly with LWP whereas the cloud emissivity is already at saturation.

Figure C shows the same observations (dark blue) and model (red) data as for A. The orange data set is the simulated LWP with a different threshold for removing precipitation: 1mm/3h instead of 0.25mm/3h. The light blue data set is the simulated LWP for all conditions (precipitation events not removed). Simulated LWP, even when all LWP events, irrespective of precipitation occurences, are included is still underestimated for all LWP bins $\geq$30g/m^2. One can also see that filtering of precipitation with the threshold of 0.25mm/3h in GEM has a large impact on LWP classes $\geq$120g/m^2 suggesting precipitation removal of cloud liquid water begins to occur efficiently at too low LWP in the GEM microphysics.

Finally, figure D shows the overestimation of the frequency of precipitation in GEM relative to observations for the range [0.75:3.25]mm/3h confirming the general overestimate of light precipitation in GEM. This problem of overestimation of light precipitation and underestimation of LWP exists for all seasons, with winter being the worst example and summer closest to observed values.

Conclusions

From these initial results, we conclude that the underestimate of LWP in GEM has two main causes. First, GEM too frequently simulates clear-sky conditions, reducing the occurence of higher LWP values. Second, even when GEM simulates clouds with higher LWP, when occurences of precipitation are removed, the majority of these LWP events are also removed, thus GEM has too many occurences of light precipitation and as a direct consequence of this, systematically too low LWP values. This underestimate of LWP can have a large impact on the simulated surface radiation budget.

Acknowledgements: Data were obtained from the ARM Program sponsored by the U.S. DOE. (www.arm.gov)

References

[1] Côté J., et al., 1998. The operational CMC-MRB global environmental multi-scale (GEM) model. Part I: Design considerations and formulation. Mon. Weather Rev.: 126, 1373-1395.

[2] Long, C. N., et al., 1999: Estimation of Fractional Sky Cover from Broadband SW Radiometer Measurements, Proc. 10th Conf. on Atmos. Rad.

Simulation of the Arctic temperature variability in the 20th century with a set of atmospheric GCM experiments

V. A. Semenov (*)

Leibniz Institute of Marine Sciences at the University of Kiel, Germany
(*) Permanent at Obukhov Institute of Atmospheric Physics RAS, Moscow, Russia
vasemenov@mail.ru

The global warming during the last four decades exhibits highest trends in the Arctic [e.g. Jones et al. 1999]. Mechanism beyond the huge Arctic surface air temperature (SAT) variations, in particular strong recent warming trend or the early 20th century warming has not yet clarified [Serreze and Francis 2006]. The positive trend of the Arctic Oscillation, local atmospheric circulation changes [Bengtsson et al. 2004], or long-term oscillation involving the North Atlantic thermohaline circulation and Arctic sea ice [Jungclaus et al. 2005] may be possible explanations.
Here, Arctic SAT in a set of simulations with the atmospheric general circulation model ECHAM5 [Roeckner et al. 2003] forced by prescribed surface conditions (sea surface temperatures, SST, and sea ice concentrations, SIC) is analyzed. The following experiments have been performed: 4 member ensemble (with different initial atmospheric conditions) using Hadley Center SST and SIC analysis for 1900-1998 (HadISST1 dataset [Rayner at al. 2003]), later cited as HadISST, and 2 member ensemble using SST data from the HadISST1 dataset for the 1961-1998 and climatological (no interannual variability) SIC for the year 1966, the year of the minimum Arctic SAT in the second half of the 20th century, to be named as ClimSIC.

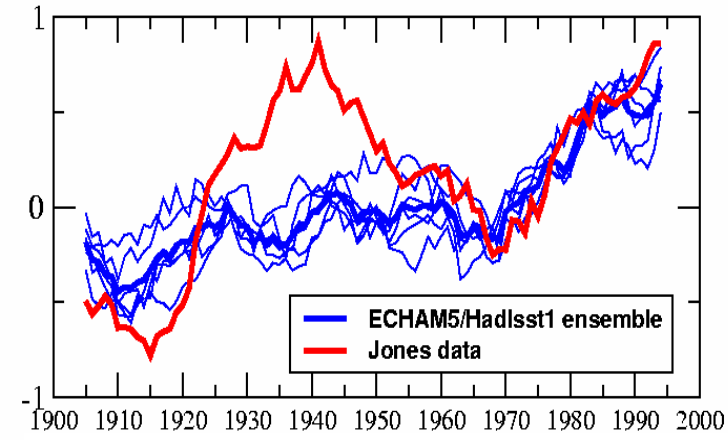

Fig. 1: Arctic winter time (Nov-Apr) SAT anomalies, K. 5 yr running means. Thick blue – ensemble mean.

Fig. 1 shows wintertime Arctic SAT (60°-90°N) anomalies as observed (Jones data) and simulated in the HadISST ensemble. The SAT trend for the last 30 years of the 20th century is very well reproduced. Some cooling of the 1950s and 1960s is also captured. However, the strong early century warming is absent. The Arctic SAT anomalies during winter time are closely related to the sea ice cover. Thus, the results imply a significant sea ice reduction in the Arctic, which is not described in the HadISST dataset. As it follows from the Fig. 2, the recent warming in the Arctic is not necessarily caused by the corresponding increase of the North Atlantic Oscillation (NAO). The model almost perfectly reproduced the SAT trend and captured some part of decadal variability (Fig. 2a) despite very weak NAO trends (Fig. 2b).

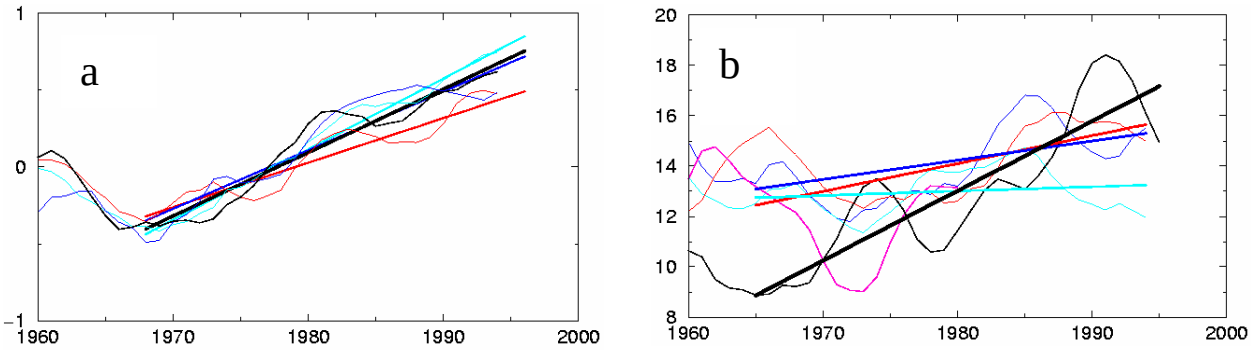

Fig. 2: observed (black) and simulated (colored, different ens. members) Arctic wintertime SAT anom., K (a), and SLP difference Lisbon-Iceland as an NAO index, mb (b). 7 yr running means and trends.

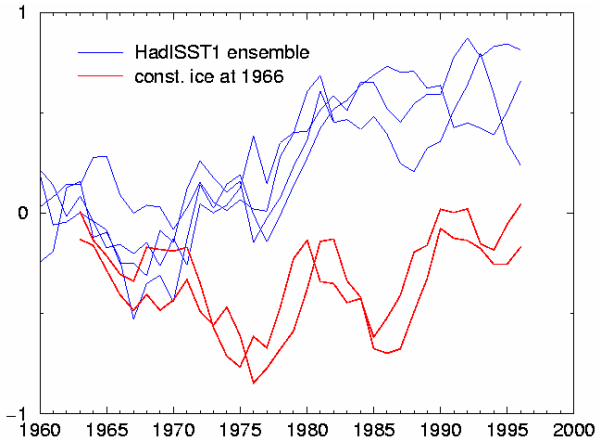

Fig. 3: Wintertime Arctic SAT anomalies in HadISST and ClimSIC simulations, K.

Without interannual variations of the Arctic sea ice cover (ClimSIC experiments) no significant Arctic SAT trend in the last decades of the 20th century is simulated (Fig. 3). All these results indicate that the sea ice cover extent in the Arctic, as a modulator of the oceanic heat loss in the marginal seas, may be the determining factor for the long-term (interdecadal) wintertime SAT variability. The sea ice analysis for the first half of the 20th century should be improved in order to represent presumably large anomaly corresponding to the early 20th century warming.

References

Jones, P. D., et al, Surface air temperature and its changes over the past 150 years. Rev. Geophys., 37, 173-199, 1999.

Bengtsson L., Semenov V.A., and O. Johannessen, The early twentieth-century warming in the Arctic - A possible mechanism. J. Climate, 17, 4045-4057, 2004.

Jungclaus J., Haak H., Latif M., and U. Mikolajewicz, Arctic-North Atlantic interactions and multidecadal variability of the meridional overturning circulation. J. Climate, 18, 4013-4031, 2005.

Rayner N.A., et al, Global analyses of sea surface temperature, sea ice, and night marine air temperature since the late nineteenth century. Journal of Geophysical Research, 108, D14, 4407, doi:10.1029/2002JD002670, 2003.

Roeckner, E., et al, The atmospheric general circulation model CHAM 5. Part I: Model description, Report 349, Max-Planck-Institute for Meteorology, Hamburg, 2003.

Serreze, M.C., and J.A. Francis, The Arctic amplification debate. Climatic Change, 76, 241-264, 2006.